Available online at www.sciencedirect.com
ScienceDirect
International Journal of Thermal Sciences 47 (2008) 609–619
International Journal of Thermal Sciences
www.elsevier.com/locate/ijts

Effect of Coriolis and centrifugal forces on turbulence and transport at high rotation and density ratios in a rib-roughened channel

A.K. Sleiti *, J.S. Kapat

Mechanical, Materials and Aerospace Department, University of Central Florida, Orlando, FL 32816, USA

Received 20 November 2006; received in revised form 29 May 2007; accepted 7 June 2007

Available online 24 July 2007

Abstract

Prediction of three-dimensional flow field and heat transfer in a two pass rib-roughened square internal cooling channel of turbine blades with rounded staggered ribs rotating at high rotation and density ratios is the main focus of this study. Rotation, buoyancy, ribs, and geometry affect the flow within these channels. The full two-pass channel with bend and with rounded staggered ribs with fillets ($e/D_h = 0.1$ and $P/e = 10$) as tested by Wagner et al. [J.H. Wagner, B.V. Johnson, R.A. Graziani, F.C. Yeh, Heat transfer in rotating serpentine passages with trips normal to the flow, ASME J. Turbomach. 114 (1992) 847–857] is investigated. Reynolds stress model (RSM) turbulence model is used for this study. To resolve the near wall viscosity-affected region, enhanced wall treatment approach is employed. RSM model was validated against available experimental data (which are primarily at low rotation and buoyancy numbers). The model was then used for cases with higher rotational numbers (0.24, 0.475, 0.74 and 1) and higher density ratios (0.13, 0.23, and 0.3). Particular attention is given to how secondary flow, Reynolds stresses, turbulence intensity, and heat transfer are affected by Coriolis and buoyancy/centrifugal forces, caused by high levels of rotation and density ratios. A linear correlation for 4-side-average Nusselt number as a function of rotation number is derived.

Introduction

Reliability of turbines is critically dependent on the temperature rise in their individual components while in operation. The creep life of turbine blades is reduced to half with every 10 to 15 °C rise in metal temperature. Also, fatigue induced failure in hot components, including blades depends on operational temperature gradients across these components. In other words, hot components design of turbines must aim to keep their operating temperatures as well as temperature gradients within some tolerable limits.

Turbines are cooled with a combination of advanced cooling techniques. However, one common technique is to have a coolant fluid (pressurized air from compressor) flowing through internal cooling channels formed within the hot components. Ribs are introduced on leading and trailing surfaces inside internal cooling channels to disturb the boundary layer and enhance the heat transfer by causing flow separation and increasing turbulence. The effect of rotation in ribbed channels is different from that in smooth channels since rotational forces are coupled with local velocity and temperature distributions. Ribs usually placed with 90 deg, 60 deg or 45 deg angles to the bulk flow. The flow inside cooling channels, in addition to the temperature loads is affected by the rotational forces (i.e. Coriolis and centrifugal). These rotational induced forces complicate the flow structure within the ducts. When performing experiments, it is very difficult to achieve conditions with high rotational speeds and density ratios and hence numerical simulations are needed. For decades researchers have investigated various aspects of internal cooling channels. Survey on the existing literature on the subject showed that studies have been performed for rotation numbers of up to 0.35 and for density ratios of up to 0.23. While in actual practice, gas turbine operates at much higher values.

Many researchers have studied stationary or low speed rotating rib-roughened channels experimentally: Webb et al. [1] investigated rib-roughened circular tubes. Han and Glicksman [2], Han and Park [3], Han et al. [4,5] and Han and Zang [6] investigated the effect of different rib cross-sectional shapes, skewed ribs and channel aspect ratio. Taslim's group

* Corresponding author.
E-mail address: asleiti@mail.ucf.edu (A.K. Sleiti).

1290-0729/$ – see front matter
doi:10.1016/j.ijthermalsci.2007.06.008

Nomenclature

De	Dean number	R	distance from axis of rotation to channel inlet
DR	density ratio	Re	Reynolds number, $\rho W_o D_h/\mu$
D_h	hydraulic diameter	r	inner radius of bend
h	heat transfer coefficient	r	radius from axis of rotation
k	thermal conductivity of coolant	k	thermal conductivity ..... w/m °C
Nu	local Nusselt number, hD_h/k	Ro	rotation number, $\Omega D_h/W_o$
Nu_o	Nusselt number in fully developed turbulent nonrotating duct flow	T_b	coolant bulk temperature
		T_o	coolant temperature at inlet
Nus	calculated Nusselt number for $Ro = 0$	T_w	wall temperature
Nur	calculated Nusselt number for $Ro > 0$	W_o	inlet velocity
P	pitch (distance between ribs)	ρ	density of air
Pr	Prandtl number	$\Delta\rho/\rho$	density ratio, $(T_w - T_o)/T_w$
R	radius from axis of rotation	μ	dynamic viscosity of coolant
S	distance in streamwise direction	Ω	rotational speed
T	local coolant temperature	θ	dimensionless temperature, $(T - T_o)/(T_w - T_o)$

Taslim [7], Taslim et al. [8], Taslim and Korotky [9], Taslim and Lengkong [10] performed heat transfer coefficient measurements on 45-degree round corner staggered ribs. The effect of a variety of rib configuration on heat transfer could be found in Taslim [11]. In the following review only rotating experimental and numerical work will be addressed.

An early experiment by Rothe and Johnson [12] showed the effect of rotation on the location of flow reattachment after a backward facing step. Wagner et al. [13] investigated orthogonal rounded-ribbed channel, with fillets in staggered arrangement. In the trailing surface of the first pass increasing Ro causes local increase in Nusselt number by 75% compared to stationary case. For high pressure surface of the first pass the heat transfer increases rapidly with increasing either the rotation number or density ratio. On the second pass leading surface the heat transfer increases by 30 to 35%. On the low pressure surfaces the heat transfer from leading first pass decreases for $Ro < 0.25$ and then, depending on density ratio, increases with increasing rotation number for larger values of density ratio. The heat transfer from the first pass trailing surface increases with density ratio. In the second pass trailing, the effects of density ratio are larger than in the first pass leading, which was attributed to uneven heat transfer coefficient distribution on the low pressure surfaces due to the combined effect of buoyancy forces and the stabilization of the near wall flow for low rotation numbers, the Coriolis-driven secondary flow, and the increases in flow reattachment lengths downstream of ribs for higher rotation numbers.

Using laser Doppler anemometry and wall pressure measurements, Iacovides et al. [14] compared the results of square U-bend staggered ribbed channel with smooth channel results for $Ro = 0.2$. They showed that the separation bubble after the turn is smaller in the ribbed channel than in the smooth one and found higher overall turbulence level and formation of a large separation bubble a long the outer wall as the flow encounters the first outer-wall rib, after the bend exit. For the low rotation number considered in that study, the turn effect was stronger than the rotational effects, which resulted in minor influence of the rotational effects immediately downstream of the turn. In more recent experimental work, Liou et al. [15] performed LDV and transient thermochromic liquid measurements on square channel with U-turn and with in line square 90-deg ribs arranged on leading and trailing surfaces. Ro was varied from 0 to 0.2 with Re fixed at 10 000. Their results showed that the rotation increased the streamwise velocity and the turbulence intensities, which leads to heat transfer enhancement. They also derived simple linear correlations between regional average Nusselt number and rotation number. Johnson et al. [16] performed heat transfer measurements on four-pass square channel with two U-turns and with 45 deg circular staggered ribs. The results showed enhancement of heat transfer rate when compared to orthogonal ribs. Rathjen et al. [17] performed experimental and numerical heat/mass transfer investigations in rotating ($Ro = 0$ and 0.1) two-pass channel with staggered 45 deg ribs.

Research relevant to predicting heat transfer in internal cooling channels is not as extensive as the experimental research. Dunn [18] gave a brief review of experimental and predicting capability work. Han et al. [19] provided both experimental and numerical review. Shih and Sultanian [20], gave a review on computations of internal and film cooling in gas turbines. Rigby [21] used k–omega turbulence model with concentration on grid structure to describe heat transfer in a ribbed channel with 180 deg bend and showed reasonable agreement with experimental results of Park et al. [22]. Prakash and Zerkle [23] performed a computation of rib-roughened rotating duct neglecting buoyancy-centrifugal effect. They used k–ε model with either wall function or a zonal approach for wall treatment. They suggested that a low-Re RSM model is necessary to capture anisotropy turbulence effect. Iacovides [24] and Iacovides et al. [14] studied velocity and heat transfer in rotating channels with orthogonal staggered ribs using low-Re Differential stress model (DSM) and effective viscosity model (EVM) with DSM performed better. Liou et al. [15] performed flow and heat trans-

fer numerical simulations using RSM turbulence model that performed reasonably well. Iacovides and Raisee [25] applied number of turbulence models, EVM and second moment type to predict the flow and heat transfer through staggered ribbed–roughened passages with U-turn. They concluded that second moment closures are necessary in order to correctly reproduce the regions of flow separation, low-*Re* turbulent models are necessary for heat transfer computations and that a low-*Re* differential stress closure yields better thermal predictions than low-*Re* EVM model. Using RSM with standard wall functions, Bonhoff et al. [26] predicted the heat transfer for both experimental cases of Wagner et al. [27] for smooth channel and Johnson et al. [16] for 45 deg rib-roughened channel using FLUENT CFD Code. The general trends of the heat transfer coefficient were predicted correctly. However, for the ribbed case, Nusselt number was overpredicted in the first pass and underpredicted in the second pass of the leading surface, the opposite for the trailing surface, and overpredicted in the inner and outer surfaces. The reason, in addition to measurements uncertainties, may be the use of wall functions approach for the near wall treatment. Murata and Mochizuki [28] studied the effect of centrifugal buoyancy on turbulent heat transfer using LES in rotating square duct with 90 and 60 deg ribs. Their results show that in the 60 deg rib case the friction factor decreased by increasing *Gr*, which was opposite to the results of the 90 deg case. The buoyancy-induced aiding flow enhanced and suppressed the Coriolis induced secondary flow in the radially outward and inward flow configurations, respectively. The predictions by Rathjen et al. [17] using k–ε model with wall function and a 2-layer approach shows significant discrepancies compared to their heat/mass transfer experimental results. Jang et al. [29] used RSM to predict flow and heat transfer for the experimental case studied by Johnson et al. [16] using one pass with *Ro* up to 0.24. They concluded that a second-moment closure is necessary to predict the high anisotropy produced by secondary flows induced by the angle ribs, rotating buoyancy and Coriolis forces. Using RSM with both standard wall functions and with enhanced wall treatment, the authors in Sleiti and Kapat [30–36] investigated the flow and heat transfer for different configurations: smooth channels with curvature at high *Ro* and DR, ribbed-roughened channels, parallel mode rotation and compared RSM to two-equation models. The results showed the advantages of using RSM with enhanced wall treatment in predicting the high anisotropy, additional secondary flows caused by high level of rotation and density ratios and the changes in Nusselt's number.

Literature review clearly reveals the need for studying the effect of high *Ro* and density ratios. The objective of this study is to perform numerical heat transfer and flow field simulation of a rib-roughened internal cooling channel of turbine blades rotating at high rotation numbers and density ratios not studied before for rib-roughened internal cooling channels configuration. Results from this study for *Nu* and pressure drop are to be compared with those for smooth channel. Particular attention would be given to how secondary flow, Reynolds stresses, turbulence intensity, and heat transfer are affected by Coriolis and buoyancy/centrifugal forces caused by high rotation (up to $Ro = 1$) and high-density ratios (up to 0.3). The results obtained are explained in view of physical interpretation of Coriolis and centrifugal forces. Reynolds stress turbulence model and enhanced near wall treatment are employed. FLUENT CFD Code, The FLUENT User's Guide [37] is used for this simulation.

Governing equations

The continuity, momentum and energy equations for a Newtonian incompressible fluid are given as:

$$\frac{\partial \rho}{\partial t} + \frac{\partial \rho U_i}{\partial x_i} = 0 \tag{1}$$

$$\frac{\partial \rho U_i}{\partial t} + \frac{\partial \rho U_i U_j}{\partial x_i} = \rho g_i + F_i - \frac{\partial P}{\partial x_i} + \frac{\partial}{\partial x_i}(2\mu S_{ij}) \tag{2}$$

$$\frac{\partial \rho E_\mathrm{o}}{\partial t} + \frac{\partial \rho U_i E_\mathrm{o}}{\partial x_i} = \rho U_i F_i - \frac{\partial q_i}{\partial x_i} + \frac{\partial}{\partial x_j}(U_i T_{ij}) \tag{3}$$

where F_i are the additional body-forces that can affect the fluid motion such as rotation, magnetic or electric field etc., and s_{ij} is the strain rate tensor, T_{ij} are the surface forces similar to the viscous and pressure terms in the momentum equations and E_o is the total internal. Assuming constant rotation velocity the extra terms due to rotation (body-force modification to the N–S equations) are

$$a_i^{ce} = \varepsilon_{ijk}\varepsilon_{klm}\Omega_j\Omega_l x_m \quad \text{and} \quad a_i^{co} = 2\varepsilon_{ijk}\Omega_j U_k \tag{4}$$

Computational approach

Reynolds Stress Model (RSM) Gibson and Launder [38], Launder [39,40], solves the Reynolds stresses, $\tau_{ij} = \overline{u_i' u_j'}$, using individual transport equations. The exact transport equations for the transport of the Reynolds stresses, may be written as follows:

$$\frac{D\tau_{ij}}{Dt} = \frac{\partial D_{T,ij}}{\partial x_k} + \frac{\partial D_{L,ij}}{\partial x_k} + P_{ij} + G_{ij} + \phi_{ij} - \varepsilon_{ij} + F_{ij} + S \tag{5}$$

where $\frac{D\tau_{ij}}{Dt} = \frac{\partial}{\partial t}(\rho\overline{u_i' u_j'}) + C_{ij}$ and $\frac{\partial}{\partial t}(\rho\overline{u_i' u_j'})$ is the local time derivative, C_{ij} the convection term, $D_{T,ij}$ the turbulent diffusion term, $D_{L,ij}$ the molecular (viscous) diffusion term, P_{ij} the stress production term, G_{ij} the buoyancy production term, ϕ_{ij} the pressure strain term, ε_{ij} the dissipation term, F_{ij} the production term by system rotation, and S the source term. Of the various terms in these exact equations, C_{ij}, $D_{L,ij}$, P_{ij}, and F_{ij} do not require any modeling. However, turbulent diffusion ($D_{T,ij}$), buoyancy production (G_{ij}), pressure strain (ϕ_{ij}), and dissipation (ε_{ij}) need to be modeled to close the equations. These terms are given as:

$$C_{ij} = \frac{\partial}{\partial x_k}\left(\rho u_k \overline{u_i' u_j'}\right)$$

$$D_{T,ij} = -\frac{\partial}{\partial x_k}\left[\rho\overline{u_i' u_j' u_k'} + \overline{p(\delta_{kj}u_i' + \delta_{ik}u_j')}\right]$$

$$D_{L,ij} = \frac{\partial}{\partial x_k}\left[\mu\frac{\partial}{\partial x_k}(\overline{u_i' u_j'})\right]$$

$$P_{ij} = -\rho\left(\overline{u_i'u_k'}\frac{\partial u_j}{\partial x_k} + \overline{u_j'u_k'}\frac{\partial u_i}{\partial x_k}\right)$$

$$G_{ij} = -\rho\beta\left(g_i\overline{u_j'\theta} + g_i\overline{u_i'\theta}\right)$$

$$\phi_{ij} = \overline{p\left(\frac{\partial u_i'}{\partial x_x} + \frac{\partial u_j'}{\partial x_i}\right)}$$

$$F_{ij} = -2\rho\Omega_k\left(\overline{u_j'u_m'}\varepsilon_{ikm} + \overline{u_i'u_m'}\varepsilon_{jkm}\right)$$

$$\varepsilon_{ij} = \frac{2}{3}\delta_{ij}(\rho\varepsilon + Y_M) \tag{6}$$

The code provides a variety of options with regard to the turbulence modeling of theses terms. The pressure-strain term, ϕ_{ij}, is modeled according to the proposals by Gibson and Launder [38] and Fu et al. [41]. Turbulent Diffusive Transport term, $D_{T,i,j}$ is modeled by the generalized gradient-diffusion model of Daly and Harlow [42]. The Fluent manual (The FLUENT User's Guide [37]) provides more details on the code and on modeling other terms.

The results for four-leg square channel with rib-roughened walls tested by Wagner et al. [13] were used in this study for comparison using two of the four legs with one U-turn. Enhanced wall treatment is used for the near wall treatment of the flow and heat transfer. For the Pressure Interpolation at the faces, the PRESTO scheme was chosen, which showed better results for cases where the pressure profile has a high gradient at the cell face.

Fig. 1 shows the duct geometry and the numerical grid generated using GAMBIT grid generator for this study. For enhanced near wall treatment, y^+ for the first cell next to a wall is taken of order unity. To resolve the near wall viscous region 17 grid points were placed in the boundary layer near all walls. The shape of each rib needs 14 grid points to be resolved. The convergence criteria for all quantities error were 10E–5 and 10E–7 for the energy equation. Unlike the experiments, uniform velocity profile was used at the entrance of the channel. At the exit, a zero normal gradient exit boundary condition is set. The density of the fluid is approximated by $\rho = \rho_o T_o/T$ to account for density variations caused by the temperature differences, while piecewise linear functions of temperature were used to account for the viscosity, thermal conductivity and specific heat properties variations.

A grid-refinement study on leading and trailing surfaces was performed using three different grid distributions of $44 \times 44 \times 880$, $64 \times 64 \times 1650$ and $82 \times 82 \times 2200$. A comparison between calculated and measured values of Nusselt number ratio on the leading surface (for $Re = 25\,000$, $Ro = 0.238$, $\Delta\rho/\rho = 0.13$) showed 6.5% maximum change in Nusselt number between $44 \times 44 \times 880$ and $64 \times 64 \times 1650$ grid distribution. Table 1 gives the grid refinement study on the trailing surface for $Re = 25\,000$, $Ro = 0.238$ and DR = 0.13. A maximum Nu enhancement of less than 1% could be achieved by increasing the grid distribution from $64 \times 64 \times 1650$ to $82 \times 82 \times 2200$. Thus it is concluded that $64 \times 64 \times 1650$ grid distribution is adequate, which resulted in 6 758 400 grid points. As a comparison, Jang et al. [29] performed a grid refinement study for the case with one pass and with 45 deg angled ribs using second moment closure. They concluded that $41 \times 41 \times 570$ grid points are adequate to resolve the whole channel.

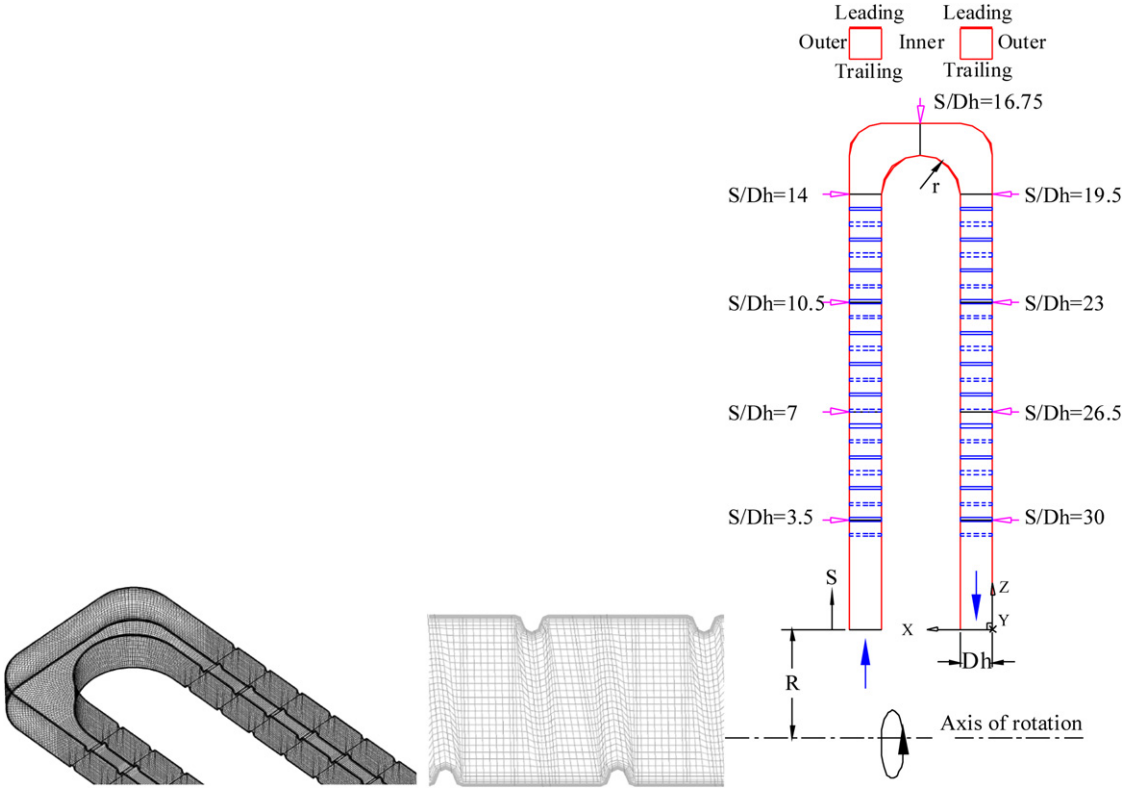

Fig. 1. Numerical grid and Geometry for two pass square channel with staggered ribs.

Table 1
Nu/Nu_o on trailing surface using different grids

Grid	S/D_h 12	Diff %	S/D_h 16	Diff %	S/D_h 24	%
$44 \times 44 \times 880$	3.48	8.5	2.55	12	1.88	10
$64 \times 64 \times 1650$	3.57	6	2.71	5.5	1.81	4.5
$82 \times 82 \times 2200$	3.58	5.8	2.69	5.3	1.8	4.2
Wagner et al. [13]	3.8	0.0	2.9	0	1.7	0

Results and discussion

The geometry of the two-pass channel is shown in Fig. 1. The four walls of the square duct are denoted as the leading, trailing, inner and outer sides. All walls are heated to a constant temperature. Eleven rounded ribs with fillet were placed on leading and trailing surfaces of every passage in a staggered arrangement with ribs on the leading surface offset upstream from those on the trailing surface by a half pitch (P). The length of every passage is $14 * D_h$, the U-turn inner diameter ($2 * r$) is $2.5 * D_h$, and the distance from axis of rotation to channel inlet (R) is $44 * D_h$ duct. The distance from the duct inlet to the first rib and from the duct outlet to last rib is $3.5 * D_h$. The rib height-to-hydraulic diameter (blockage ratio) is 0.1 and the rib pitch-to-height ratio is 10. In this study, rotation numbers considered are 0.0, 0.238, 0.475, 0.74 and 1. Density ratios of 0.13, 0.229, and 0.3 which correspond to wall temperature of 344, 389, and 428 K, respectively with Reynolds number fixed to 25 000 and operating pressure to 10 atm. Nusselt numbers were normalized with a smooth tube correlation (Kays and Crawford [43]) for fully developed, nonrotating, turbulent flow:

$$Nu_o = 0.0176 Re^{0.8} \tag{7}$$

The coolant temperature is T_o (i.e., $\theta = (T - T_o)/T_w - T_o) = 0$) at the duct entrance and the wall temperature was kept constant at $T = T_w(\theta = 1)$ for all sidewalls. A comparison between the calculated and measured Nusselt number ratio was performed for rotation number of 0.0, 0.238 and 0.35 at coolant-to-wall density ratio ($\Delta\rho/\rho$) of 0.13 and is given in Fig. 2. The predicted Nusselt number using RSM with enhanced near wall treatment are in good agreement with measured data to within 10%. At the entrance, the predictions for all cases are less than

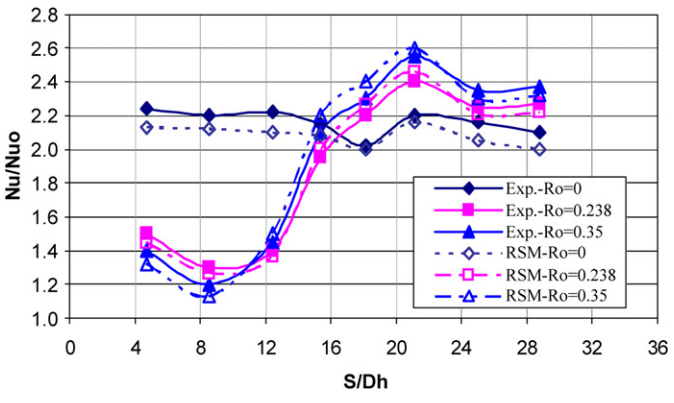

Fig. 2. Predicted and measured, Wagner et al. [13] Nusselt number ratios on leading surface; $Re = 25\,000$, DR = 0.13.

the measured. This may attributed to the difference between the experimental and numerical inlet boundary conditions.

Temperature and streamwise velocity profiles and secondary flows

Study was performed for rotation numbers of 0, 0.475 and 1 at 0.13 DR and for $Ro = 1$ at DR = 0.13, 0.23 and 0.3. The Reynolds number and radius ratio R/D_h were held constant at 25 000 and 44, respectively. Fig. 3 provides the streamwise velocity vectors and temperature distribution in a vertical cross-section at the center of the 1st pass, U-turn and 2nd pass, respectively and Fig. 4 shows the secondary flow patterns and temperature contours, where each figure is viewed from upstream. In the first pass, for $Ro = 0$ (not shown) the Reynolds stress anisotropy generate secondary flow at the corners. The outward flow impinges into the ribs which causes a small region of flow separation in front and after each circular rib on both leading and trailing surfaces. Increasing Ro to 0.475 caused the formation of large thin vortices between ribs in the leading surface as a result of the effect of the ribs and the buoyancy force that decelerate the slow momentum hotter fluid near the leading surface. The centrifugal force accelerates the colder fluid near the trailing surface where the small vortices become clearer and the reattachment length increases. At this level of rotation ($Ro = 0.475$) two Coriolis induced vortices and two additional vortices because of ribs, appear near the trailing surface at location $S/D_h = 8.5$. At higher rotation numbers, $Ro = 0.74$ and $Ro = 1$, the main flow completely gets separated near the leading side. Coriolis and buoyancy/centrifugal effects are much stronger at high Ro, causing the small vortices near the leading surface to become large vortices in the stream wise direction and the small vortices at the trailing rib-back to become wider and those at the trailing rib-front shorter. Increasing DR to 0.23 tends to decrease the size of vortices near the leading side. In the U-turn the flow separates at $Ro = 1$ and DR = 0.13 and 0.23. Two vortices are formed in the U-turn ($S/D_h = 16.75$), as a results of the combined effect of cross-stream Coriolis forces and high-pressure gradients. In the second pass, where the Coriolis is acting toward the leading surface and buoyancy aligned with streamwise flow, high rotation (at $Ro = 1$) accelerates the flow and tends to suppress the vortices in front of the ribs shortly after the U-turn and then, downstream a flow circulation is observed between ribs on the trailing surface. Increasing DR to 0.23 causes more flow acceleration and tends to suppress the vortices behind the ribs. Fig. 3 and 4 clearly show that as DR increases the temperature difference between walls and fluid becomes more than that of cases with lower DR.

Turbulence anisotropy

The complexity of the flow inside internal cooling channels (ribs, U-turn, rotation, etc.) generates turbulence anisotropy. Thus the turbulence model employed to solve such flow phenomena must be capable of capturing anisotropic turbulence effects. Fig. 5 depicts the ratio of the Reynolds stress normal components in the first pass, U-turn, and second pass. In the

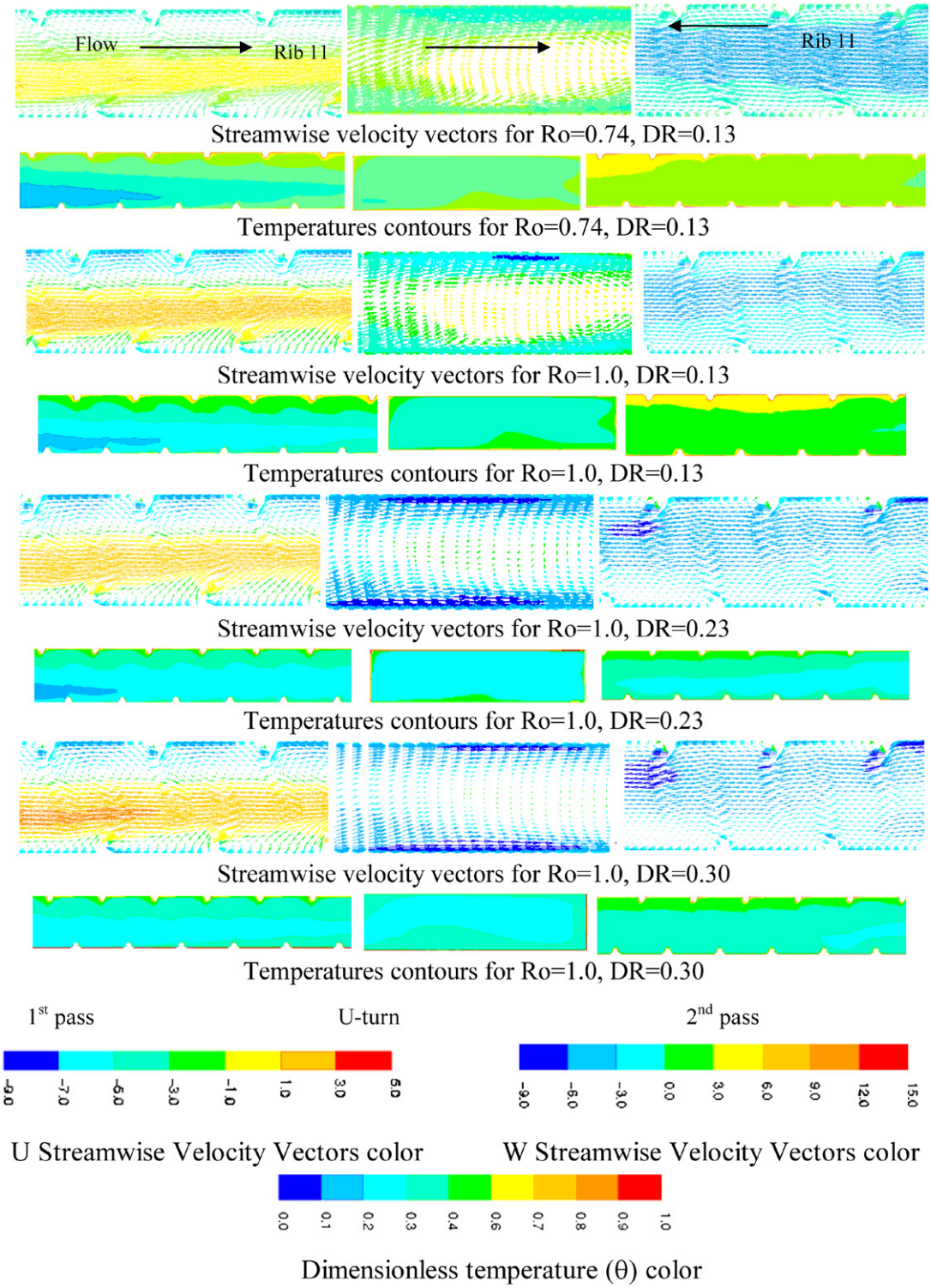

Fig. 3. Streamwise velocity vectors (W in the 1st and 2nd pass and U in U-turn) and θ contours.

first pass, where the Coriolis force is directed toward the trailing surface such that the streamwise velocity profiles are skewed toward the trailing wall. The rib generated shear layer on the trailing side and the high velocity gradients associated with skewed velocity profiles caused high turbulence anisotropy, approximately having values of 0.4–1.9 at $Ro = 0.475$ and DR = 0.13, 0.3–1.6 for $Ro = 1$ and DR = 0.13 and of 0.32–1.9 for $Ro = 1$ and DR = 0.23 near the leading surface. In the second pass, the turbulence anisotropy has values of 0.4–1.8 at $Ro = 0.475$ and DR = 0.13, 0.4–1.8 for $Ro = 1$ and DR = 0.13 and of 0.27–1.7 for $Ro = 1$ and DR = 0.23 near the trailing surface. In the U-turn, the turbulence anisotropy has values of 0.55–1.8 at $Ro = 0.475$, 0.5–1.7 for $Ro = 1$, DR = 0.13 and of 0.4–1.8 for $Ro = 1$, DR = 0.23 near the trailing surface. As a com-

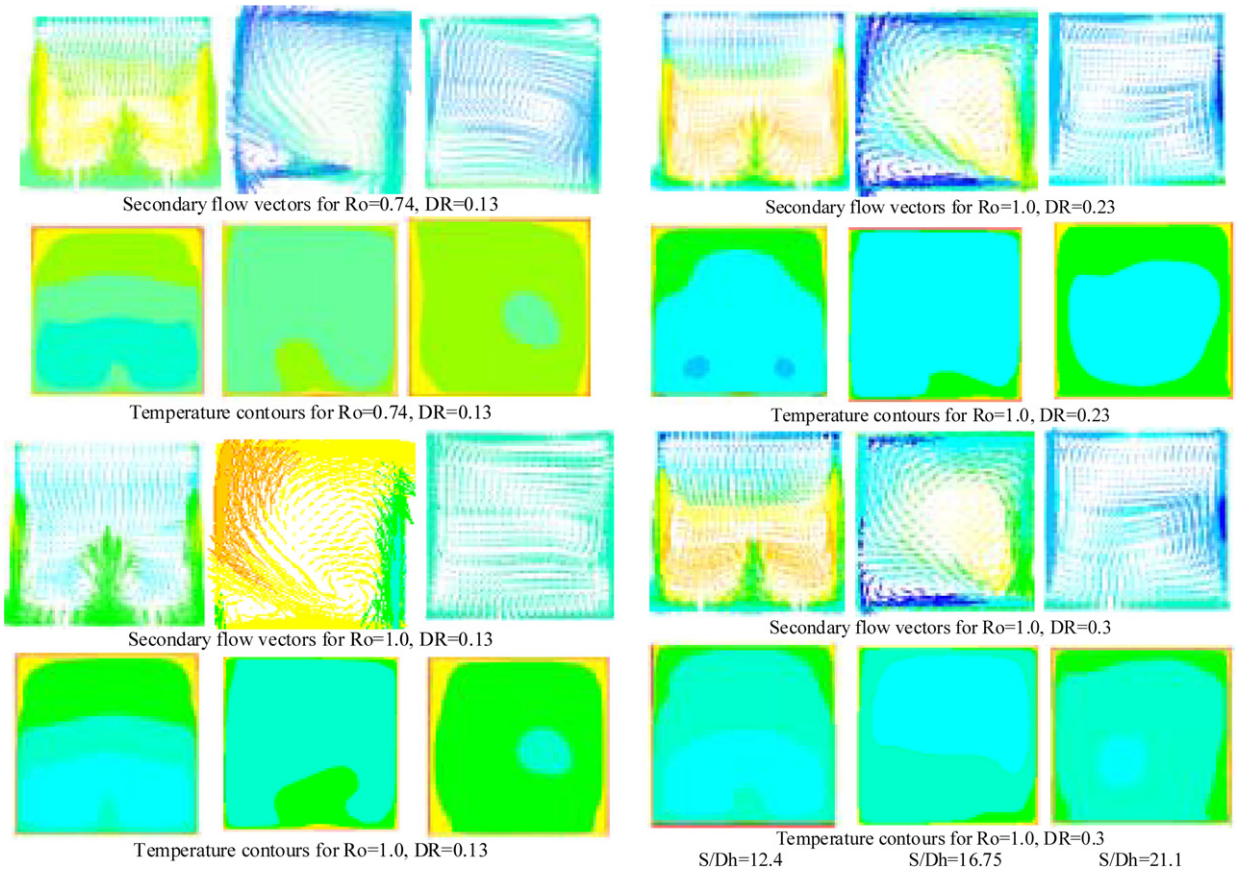

Fig. 4. Secondary flow vectors (colored by streamwise velocity, W in the 1st and 2nd pass and U in U-turn) and θ contours.

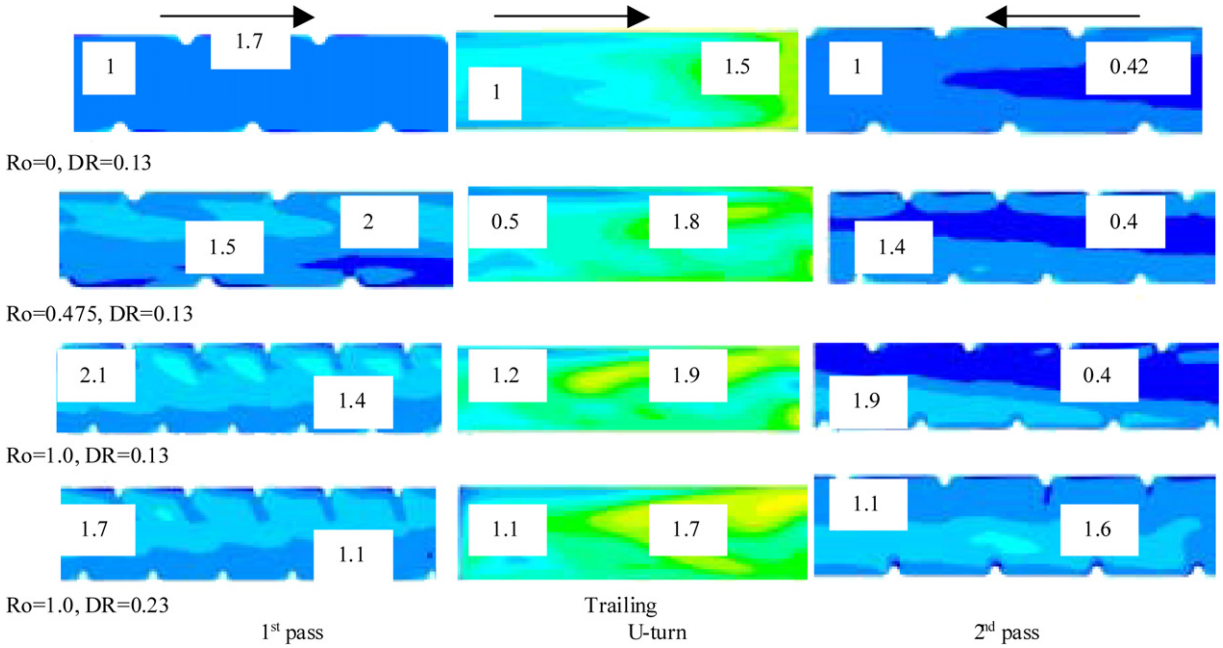

Fig. 5. Turbulence anisotropy in terms of $w'w'/v'v'$ contours in the first and second pass and in terms of $u'u'/v'v'$ in the U-turn.

parison, Liou et al. [15] in their experimental study of flow and heat transfer in a rotating two-pass square channel with 90 deg in-line square ribs on leading and trailing surfaces reported turbulence anisotropy, also in terms of the ratio of the Reynolds stress normal components, of 1.8–2.2, 1.8–2.8 and 1.3–2.4 in the first pass, U-turn, and second pass, respectively for $Ro = 0.2$. The results from our study show that high rotation and density ratios, although suppresses turbulence in general

trend but it also tend to redistribute these intensities resulting on large low intensities and small high intensities regions.

The influence of F_{ij} on dynamics

The system rotation at angular velocity Ω^* is manifested in the velocity fluctuation equation by the appearance of a Coriolis force term, $-2(\Omega^* \times V)$. The additional forces that are acting on the flow are:

Coriolis force: $f_{co} = -2\rho(\Omega \times V)$, which in this case yields: $f_{co} = -2\rho[j(\Omega w) - k(\Omega v)]$. In the first pass the Coriolis force, due to W velocity component acts toward trailing surface (in second pass vice versa). In the U-turn the Coriolis force due to $+V$ and $-V$ velocity components acts towards outer and inner surfaces, respectively.

Centrifugal force: $f_{ce} = -\rho[\Omega \times (\Omega \times r)]$, which yields: $f_{ce} = k(\rho\Omega^2 r)$. In the first, second passes and in the U-turn the centrifugal force acts toward positive z direction a way from axis of rotation.

The derived equation for the production term by system rotation is given by:

$$F_{ij} = -2\rho\Omega_k\left(\overline{u'_j u'_m}\varepsilon_{ikm} + \overline{u'_i u'_m}\varepsilon_{jkm}\right) \tag{8}$$

With a rotation vector $\Omega^* = (-\Omega i + 0j + 0k)$, it follows from Eq. (8) that the Reynolds stresses equations contain additional terms as shown in Table 2.

When $\overline{w'w'} > \overline{v'v'}$, F_{32} becomes negative, in which case it acts to add to Reynolds shear stress on the trailing surface where ($\overline{w'v'} < 0$) and decrease it on the leading surface if no density ratio is involved (flow without heating). Enhanced Reynolds shear stress may be associated with high turbulence activity. If the fluid is heated, the buoyancy becomes very important factor that affects the Reynolds stresses.

Reynolds shear stress components

The shear stresses, $\overline{v'w'}$, play a dominant role in the theory of mean momentum transfer by turbulent motion. They are depicted in Fig. 6 (normalized with Wo^2) in the first pass, U-turn and second pass. In the first pass, high rotation (strong Coriolis), and buoyancy increased shear stresses near the trailing surface (with minus sign) and also increase them near the leading surface (with positive sign) compared to stationary case. In the U-turn at $Ro = 1$, two regions are predicted with high shear stress; 0.05 near the leading and -0.065 near the trailing surfaces. Increasing density ratio to 0.23 caused an increase of $\overline{u'w'}$ to 0.085 near leading and -0.12 near trailing, respectively.

Table 2
The influence of F_{ij} on dynamics

1st pass			U-turn			2nd pass		
i, j	*Re* stress	F_{ij}	i, j	*Re* stress	F_{ij}	i, j	*Re* stress	F_{ij}
3,3	$\overline{w'w'}$	$4\rho\Omega\overline{w'v'}$	1,1	$\overline{u'u'}$	0	3,3	$\overline{w'w'}$	$4\rho\Omega\overline{w'v'}$
2,2	$\overline{v'v'}$	$-4\rho\Omega\overline{v'w'}$	2,2	$\overline{v'v'}$	$-4\rho\Omega\overline{v'w'}$	2,2	$\overline{v'v'}$	$-4\rho\Omega\overline{v'w'}$
3,2	$\overline{w'v'}$	$2\rho\Omega(\overline{v'^2} - \overline{w'^2})$	1,2	$\overline{u'v'}$	$-2\rho\Omega\overline{u'w'}$	3,2	$\overline{w'v'}$	$2\rho\Omega(\overline{v'^2} - \overline{w'^2})$

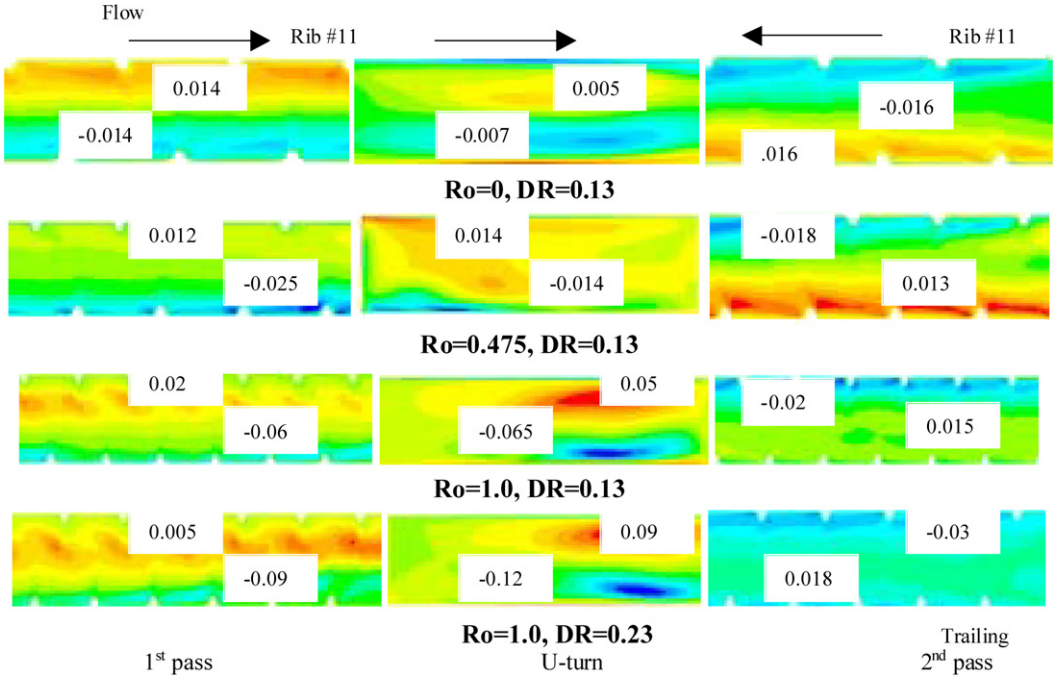

Fig. 6. Reynolds shear stresses in terms of $v'w'/Wo^2$ contours in the first and second pass and in terms of $u'v'/Wo^2$ in the U-turn. (values shown are the (+ve and −ve) maximum).

In the second pass shear stresses increased near the leading surface as *Ro* and DR increases. Near the trailing surface, $\overline{u'w'}$ first decreases by increasing rotation number to 0.475 then increases as *Ro* and DR increase. Increasing DR to 0.23 caused further increase in shear stresses near the leading and more increase near the trailing with minus sign. In summary, the shear stresses are increasing by increasing both *Ro* and DR in the first and second passages and in the U-turn. The effect of this trend on Nu is to be addressed next.

Nusselt number

Nu distribution in a ribbed-roughened channel is different from that in smooth walls channel. The local *Nu* is very high on top of the ribs and much smaller between the ribs as shown by Fig. 7. However, in order to study the effect of increasing rotation number and density ratio on heat transfer distribution, Nusselt number is calculated at 9 locations on the leading, trailing, inner and outer surfaces for *Ro* of up to 1 and DR of up to 0.3. Note that this approach does not represent the actual distribution of *Nu*, but rather gives a comparison between different levels of *Ro* and DR. Calculation of Nusselt number is based on the mass weighted average bulk temperature at every section of the 9 locations. The results are shown in Fig. 8. Note that the heat transfer coefficients in Wagner et al. [13] were based on the projected area rather than the actual heat transfer surface area due to the rib geometry, where the actual heat transfer area is 1.15 times the projected area. On the leading surface, for every level of rotation, *Nu* decreases up to $S/D_h = 14$ then starts to increase in the U-turn up to $S/D_h = 15.75$. Then *Nu* decreases and again increases in the second pass. Increasing DR to 0.23 increased *Nur* slightly on the first and second pass but decreased *Nur* on the U-turn region. Increasing DR to 0.3 did not change *Nur* much. On the trailing surface the opposite is observed. *Nur* increases rapidly in the first pass as *Ro* increases and then increasing DR *Nur* decreases. In the U-turn, *Nur* increases as *Ro* increases and as DR increases. In the second pass, increasing DR caused a slight decrease in *Nur*. On the inner surface *Nur* increased for every *Ro* up to $S/D_h = 10$ then decreased slightly then picked up its maximum value on the U-turn region after which it decreases to its minimum values. Increasing *Ro* caused an increase on *Nur* while increasing DR decreased *Nur* for all location on the inner surface. On the outer surface, increasing *Ro* increases *Nur* in the first pass and in the U-turn, while in the

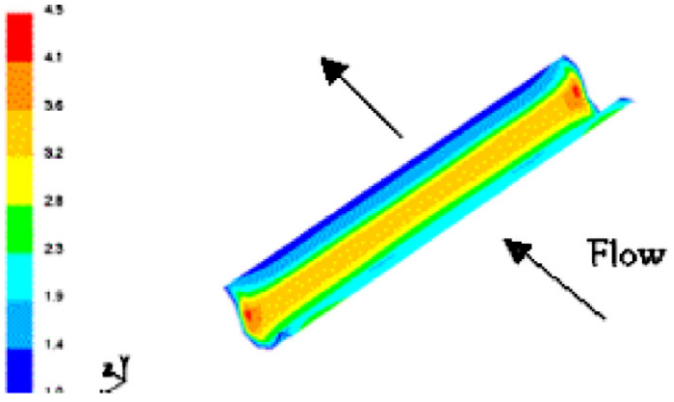

Fig. 7. Nu/Nu_o distribution on rib #6 on the leading surface of the first pass ($Ro = 1.0$, DR = 0.23).

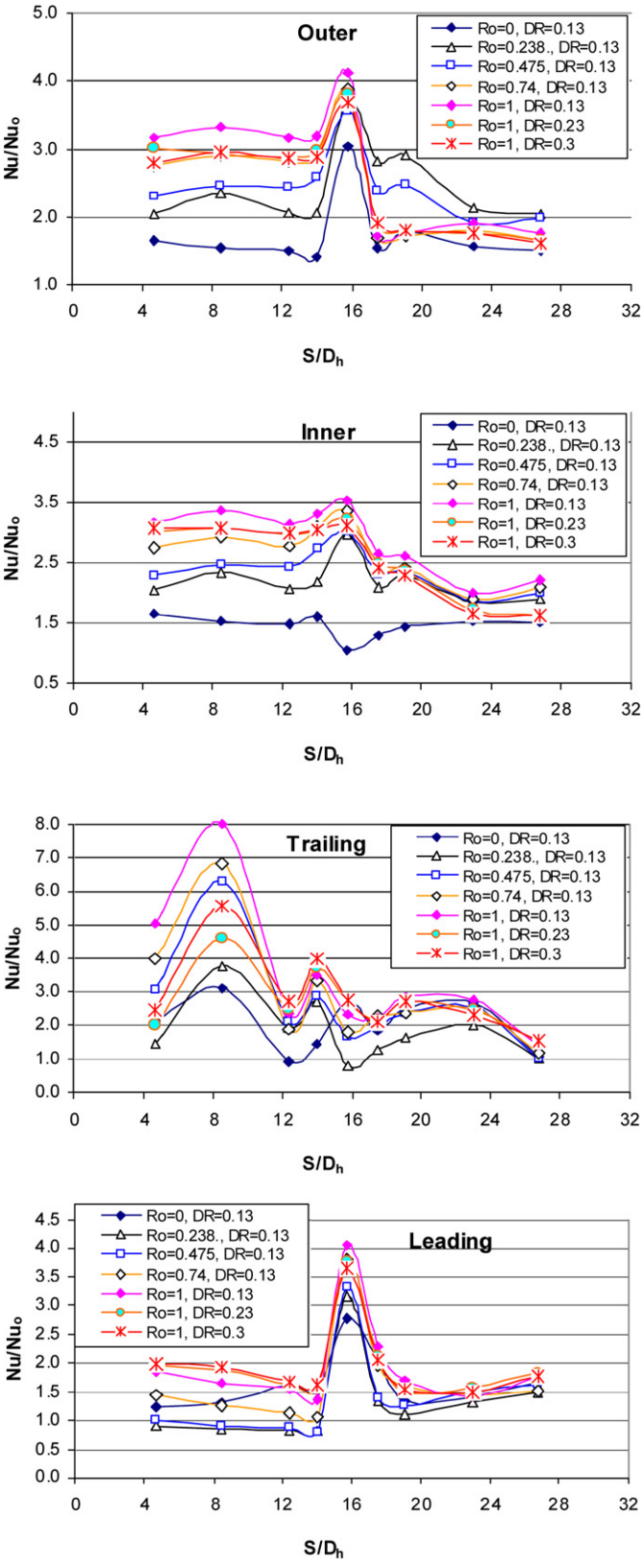

Fig. 8. Effect of increasing *Ro* and DR on local Nu/Nu_o on all four surfaces.

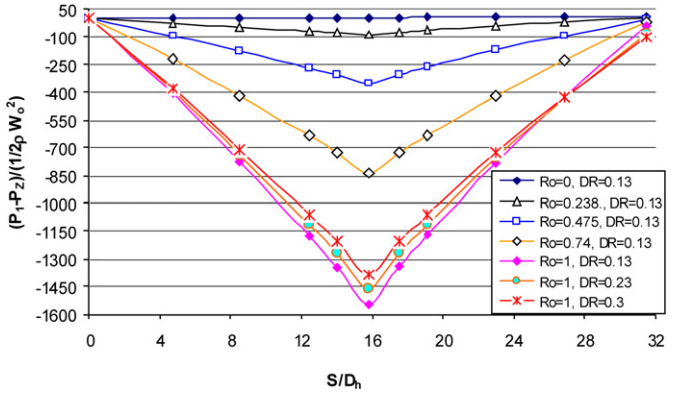

Fig. 9. Mass weighted total pressure drop.

second pass, *Nur* decreases by increasing *Ro*. Increasing DR decreases *Nur* slightly in all locations. The maximum increase in *Nur* was found on the first pass and the U-turn region, while the maximum decrease was found on the second pass. From these results it has been observed that the 4-side-average *Nur* increases linearly with *Ro*. Thus it is possible to derive correlation for *Nur*/*Nus* as a function of rotation number and another correlation as a function of density ratio for every surface (i.e. leading, trailing, inner and outer) or for the whole channel. Such correlation for the whole channel was derived based on *Ro* of 0.24, 0.35, 0.475, 0.74 and 1 and it's given as:

$$Nur/Nus = 0.613 * Ro + 1 \tag{9}$$

The variation of *Nur* with DR is not significant at high rotation numbers. The decrease in *Nur* as DR increases is due to the fact that although the wall heat flux increases, the increase in the difference between wall and fluid bulk temperature is more. At low rotation numbers (up to $Ro = 0.35$), increasing density ratio caused an increase in *Nu* on the leading and trailing surfaces at all locations of the channel. This behavior of *Nu* is confirmed in the experimental results by Wagner et al. [13] for *Ro* up to 0.475 and DR up to 0.23. At high *Ro*, when DR increases the Reynolds shear stresses increase near both trailing and leading surfaces, while *Nur* decreases. The explanation for this behavior of *Nur* is that by increasing DR the fluid density decreases significantly such that the increase in Reynolds shear stresses does not compensate that decrease in density to enhance the heat transfer.

Total pressure drop

Fig. 9 shows the mass weighted average pressure drop across the channel. In the first pass the total pressure increases as *Ro* increases to reach the maximum value in the U-turn, then starts to decrease in the second pass. Increasing DR decreases the total pressure as the density of the fluid is decreasing.

Conclusions

Prediction of heat transfer and flow field of a rib-roughened internal cooling channel of turbine blades rotating at high rotation numbers (up to 1) and density ratios (up to 0.3) is performed, the results show the following:

RSM turbulence model and enhanced near wall treatment provided accurate predictions for *Nu* when compared to experimental data.

At $Ro = 1$ large vortices are formed near the leading surface in the stream wise direction. Increasing DR to 0.23 tends to decrease the size of vortices. In the U-turn the flow separates at $Ro = 1$ and DR = 0.13 and 0.23 and two new vortices are formed.

The rib generated shear layer on the trailing side and the high velocity gradients associated with skewed velocity profiles caused high turbulence anisotropy, having values of $W'W'/V'V'$ from less than 1 to more than 2.

High rotation (strong Coriolis), and buoyancy increase shear stresses near the trailing and leading surfaces compared to stationary case. In the U-turn at $Ro = 1$, two regions are predicted with high shear stress; near the leading and near the trailing surfaces. Increasing density ratio caused an increase near leading and trailing surfaces.

Increasing rotation number enhances heat transfer, while increasing density ratio to 0.3 at high *Ro* did not or in some locations slightly decreases *Nur*.

4-side-average *Nur* correlates with *Ro* linearly, where a linear correlation for *Nur*/*Nus* as a function of rotation number is derived for the parameters studied, i.e., $Re = 25\,000$, $R/D_h = 44$, *Ro* from 0 to 1, and DR of 0.13.

References

[1] R.L. Webb, E.R.G. Eckert, J. Goldstein, Heat transfer and friction in tubes with roughness, Int. J. Heat Mass Transfer 14 (1971) 601–617.
[2] J.C. Han, L.R. Glicksman, Turbulent heat and mass transfer from a wall with parallel roughness ridges, Int. J. Heat Mass Transfer 21 (1978) 1143–1156.
[3] J.C. Han, J.S. Park, Developing heat transfer in a rectangular channels with rib turbulators, Int. J. Heat Mass Transfer (1988) 183–195.
[4] J.C. Han, J.S. Park, C.K. Lei, Heat transfer enhancement in channels with promoters, J. Eng. Gas Turbines Power 107 (1985) 628–635.
[5] J.C. Han, Y.M. Zang, C.P. Lee, Augmented heat transfer in square channels with parallel, crossed, and V-shaped angled ribs, J. Heat Transfer 113 (1991) 590–596.
[6] J.C. Han, Y.M. Zang, Augmented heat transfer in square channels with parallel broken, and V-shaped ribs, J. Heat Transfer 113 (1992) 590–596.
[7] M.E. Taslim, 45-degree round-corner rib heat transfer coefficient measurements in a square channel, J. Turbomachinery 121 (1999) 1–9.
[8] M.E. Taslim, T. Li, S.D. Spring, Measurements of heat transfer coefficients and friction factors in passages rib-roughened in all walls, ASME J. Turbomachinery 120 (1999) 256–570.
[9] M.E. Taslim, G.J. Korotky, Low-aspect ratio rib heat transfer coefficient measurements in square Channel, ASME J. Turbomachinery 120 (1998) 831–838.
[10] M.E. Taslim, A. Lengkong, 45 deg. staggered rib heat transfer coefficient measurements in a square channel, ASME J. Turbomachinery 120 (1998) 571–580.
[11] M.E. Taslim, Aero-thermal performance of internal cooling systems in turbomachines, VKI Lecture Series 2000-03, 2000.
[12] P.H. Rothe, J.P. Johnson, Free shear layer behavior in rotating systems, ASME J. Fluids Engrg. 101 (1979) 117–120.
[13] J.H. Wagner, B.V. Johnson, R.A. Graziani, F.C. Yeh, Heat transfer in rotating serpentine passages with trips normal to the flow, ASME J. Turbomachinery 114 (1992) 847–857.
[14] H. Iacovides, D.C. Jackson, H. Ji, C. Kelemenis, E.B. Launder, K. Nikas, LDA study of the flow development through orthogonally rotating U-bend

of strong curvature and rib roughened walls, ASME J. Turbomachinery 120 (1998) 386–391.
[15] T.M. Liou, M.-Y. Cheng, M.-H. Tsai, Fluid flow and heat transfer in a rotating two-pass square duct with in-line 90-deg ribs, J. Turbomachinery 124 (2002) 260–268.
[16] B.V. Johnson, J.H. Wagner, G.D. Stuber, F.C. Yeh, Heat transfer in rotating serpentine passages with trips skewed to the flow, J. Turbomachinery 116 (1994) 113–123.
[17] L. Rathjen, D.K. Hennecke, C. Sivade, K. Semmler, Detailed experimental and numerical heat/mass transfer investigations in a rotating two-pass coolant channel with staggered 45 deg ribs, in: Proc. 9th Int. Symp. on Transport Phenomena and Dynamics of Rotating Machinery (ISROMAC-9-HT034), Honolulu, Hawaii, USA, 2002.
[18] M.G. Dunn, Convective heat transfer and aerodynamics in axial flow turbines, J. Turbomachinery 123 (2001) 637–686.
[19] J.C. Han, S. Dutta, E. Srinath, Gas Turbine Heat Transfer and Cooling Technology, Taylor & Francis, New York, 2000.
[20] T.I.-P. Shih, B. Sultanian, Computations of Internal and Film Cooling, WIT Press, Aouthhampton, Ashurst, 2001.
[21] D.L. Rigby, Prediction of heat and mass transfer in a rotating ribbed coolant passage with a 180 degree turn, ASME Paper No. 98-GT-329, 1998.
[22] C.W. Park, S.C. Lau, R.T. Kukreja, Heat/mass transfer in a rotating two-pass square channel with transverse ribs, J. Thermophys. Heat Transfer 11 (1997) 8–16.
[23] C. Prakash, R. Zerkle, Prediction of turbulent flow and heat transfer in a ribbed rectangular duct with and without rotation, ASME J. Turbomachinery 117 (1995) 255–261.
[24] H. Iacovides, The computation of turbulent flow through stationary and rotating U-bends with rib-roughened surfaces, in: 10th International Conference on Numerical Methods in Laminar and Turbulent Flows, Swansea, 1997.
[25] H. Iacovides, M. Raisee, Recent progress in the computation of flow and heat transfer in internal cooling passages of turbine blades, Int. J. Heat Fluid Flow 20 (1999) 320–328.
[26] B. Bonhoff, U. Tomm, B. Johnson, I. Jennions, Heat transfer predictions for rotating u-shaped coolant channels with skewed ribs and with smooth walls, in: Int. Gas Turbine & Aero-Engine Congress and Exhibition, 1997.
[27] J.H. Wagner, B.V. Johnson, T. Hajek, Heat transfer in rotating passages with smooth walls and radial outward flow, ASME J. Turbomach. 113 (1991) 42–51.
[28] A. Murata, S. Mochizuki, Effect of centrifugal buoyancy on turbulent heat transfer in an orthogonally rotating square duct with transverse or angled rib turbulators, Int. J. Heat Mass Transfer 44 (2001) 2739–2750.
[29] Y.-J. Jang, H.-C. Chen, J.-C. Han, Flow and heat transfer in a rotating square channel with 45 deg angled ribs by Reynolds stress turbulence model, J. Turbomachinery 123 (2001) 124–132.
[30] A.K. Sleiti, J.S. Kapat, Effect of Coriolis and centrifugal forces at high rotation and density ratios, J. Thermophys. Heat Transfer 20 (2006) 67–79.
[31] A.K. Sleiti, J.S. Kapat, Effect of Coriolis and centrifugal forces on turbulence and transport at high rotation and buoyancy numbers in smooth internal cooling channels, in: 42nd AIAA Aerospace Sciences Meeting and Exhibit, Reno, Nevada, 2004.
[32] A.K. Sleiti, J.S. Kapat, Effect of Coriolis and centrifugal forces on turbulence and heat transfer at high rotation and buoyancy numbers in rib-roughened internal cooling channel, American Society of Mechanical Engineers (ASME) Paper, GT2004-53018, Vienna, Austria, 2004.
[33] A.K. Sleiti, J.S. Kapat, Fluid flow and heat transfer in rotating curved duct at high rotation and density ratios, J. Turbomachinery 127 (2005) 659–667.
[34] A.K. Sleiti, J.S. Kapat, Comparison between EVM and RSM turbulence models in predicting flow and heat transfer in rib-roughened channels, J. Turbulence 7 (2006) 1–21.
[35] A.K. Sleiti, J.S. Kapat, Comparison between EVM and RSM turbulence models in predicting flow and heat transfer in RIB-roughened channels, in: Proceedings of the ASME Heat Transfer/Fluids Engineering Summer Conference 2004, HT/FED 2004 2 A, 2005, pp. 531–542.
[36] A.K. Sleiti, J.S. Kapat, Heat transfer in channels in parallel-mode rotation at high rotation numbers, J. Thermophys. Heat Transfer 20 (2006) 748–753.
[37] The FLUENT User's Guide, Version 6.2.
[38] M.M. Gibson, B.E. Launder, Ground effects on pressure fluctuations in the atmospheric boundary layer, J. Fluid Mech. 86 (1978) 491–511.
[39] B.E. Launder, Second-moment closure: Present and future, Int. J. Heat Fluid Flow 10 (1989) 282–300.
[40] B.E. Launder, Introduction to Modeling of Turbulence, von Karman Institute for Fluid Dynamics, 1985.
[41] S. Fu, B.E. Launder, M.A. Leschziner, Modeling strongly swirling recirculating jet flow with Reynolds-stress transport closures, in: Sixth Symposium on Turbulent Shear Flows, Toulouse, France, 1987.
[42] B.J. Daly, F.H. Harlow, Transport equations in turbulence, Phys. Fluids 13 (1970) 2634–2649.
[43] W.M. Kays, M.E. Crawford, Convective Heat and Mass Transfer, third ed., McGraw–Hill, 1993.